PHILOSOPHICAL TRANSACTIONS OF THE ROYAL SOCIETY A

Phil. Trans. R. Soc. A (2008) **366**, 705–728
doi:10.1098/rsta.2007.2123
Published online 18 October 2007

Investigation of a multi-ball, automatic dynamic balancing mechanism for eccentric rotors

By K. Green*, A. R. Champneys, M. I. Friswell and A. M. Muñoz†

Bristol Laboratory for Advanced Dynamics Engineering, University of Bristol, Queen's Building, University Walk, Bristol BS8 1TR, UK

This paper concerns an analytical and experimental investigation into the dynamics of an automatic dynamic balancer (ADB) designed to quench vibration in eccentric rotors. This fundamentally nonlinear device incorporates several balancing masses that are free to rotate in a circumferentially mounted ball race. An earlier study into the steady state and transient response of the device with two balls is extended to the case of an arbitrary number of balls. Using bifurcation analysis allied to numerical simulation of a fully nonlinear model, the question is addressed of whether increasing the number of balls is advantageous. It is found that it is never possible to perfectly balance the device at rotation speeds comparable with or below the first natural, bending frequency of the rotor. When considering practical implementation of the device, a modification is suggested where individual balls are contained in separate arcs of the ball race, with rigid partitions separating each arc. Simulation results for a partitioned ADB are compared with those from an experimental rig. Close qualitative and quantitative match is found between the theory and the experiment, confirming that for sub-resonant rotation speeds, the ADB at best makes no difference to the imbalance, and can make things substantially worse. Further related configurations worthy of experimental and numerical investigation are proposed.

Keywords: Jeffcott rotor; imbalance; autobalancer; bifurcation; vibro-impact; multistability

1. Introduction

Imbalance in rotating machinery is a common source of vibration in many applications. Owing to the centre of mass of the rotating component not being located at the centre of rotation, such *eccentric rotors* undergo periodic oscillation known as *whirl* (Jeffcott 1919). To limit this vibration, rotors are typically balanced by either using fixed static masses added to the rotor, or conversely by machining away small mass from the rotor, during the

* Author and address for correspondence: Theoretical Physics, FEW, Vrije Universiteit, De Boelelaan 1081, 1081HV Amsterdam, The Netherlands (k.green@few.vu.nl).
† Present address: Escuela Técnica Superior de Ingenieros, University of Seville, Camino de los Descubrimientos s/n, Sevilla 41092, Spain.

One contribution of 8 to a Theme Issue 'Experimental nonlinear dynamics I. Solids'.

manufacturing process. However, such balancing cannot compensate for changes in imbalance that occur post-production or as a result of operating conditions. Thus, frequent field balancing is required in many applications. Furthermore, this addition (subtraction) of static mass cannot account for a dynamic imbalance. One example of a dynamic imbalance is found in a washing machine, i.e. one cannot predict, *a priori*, where the washing will accumulate during the wash cycle (Adolfsson 2001).

Such dynamic imbalance has inspired the use of self-compensating, automatic dynamic balancing (ADB) mechanisms for eccentric rotors. The principal idea behind the ADB is that the balancing balls are subjected to a *driving force* caused by an *apparent* centripetal force acting from the offset centre of mass to each ball. When the speed of rotation is below the first resonance, this driving force pushes the balls towards the imbalance, thus moving the centre of mass away from the centre of rotation. However, when the speed of rotation is greater than the first resonance, the driving force pushes the balls to the opposite side of the rotor than the imbalance, thus moving the centre of mass towards the centre of rotation. Viscous damping in the ball race causes energy dissipation, allowing the balls to come to rest in asymptotically stable steady-state positions.

The ADB first received attention as early as 1904, with the first theoretical investigation, accompanied by some experiments, undertaken by Thearle (1932). In this paper, there is also a discussion on why an ADB consisting of a fluid, in place of solid weights, would not work. Further theoretical investigations can be found in Sharp (1975) and Majewski (1987), in which the results of a linear stability analysis show that complete balance is possible for sufficiently high rotation speeds. Moreover, Ryzhik *et al.* (2004*a*) showed that even if partial balance can only be achieved, an ADB increasingly reduces vibration as the rotation speed is increased. There are several commercial implementations of ADBs, with a number of patents granted from 1961 onwards (see Lee & Van Moorhem 1996). Applications include optical disc drives, in which the aim is to achieve higher operating speeds without losing tracking performance (Kim & Chung 2002; van de Wouw *et al.* 2005), and balancing of machine tools, such as lathes, angle grinders and cutting tools (Rajalingham & Rakheja 1998). However, the ADB idea has not been more generally adopted, not least because the problem is fundamentally nonlinear, and is extremely sensitive to perturbation. Thus, while the ADB can completely quench whirl oscillations at some rotation speeds and for some initial conditions, it can also make the imbalance significantly worse.

Only recently have fully nonlinear analyses of the autobalancer been undertaken. Based on a Lagrangian description of the equations of motion, steady-state bifurcation studies were carried out by Chung & Ro (1999) and by Adolfsson (2001), who identified regions in parameter space where stable rotating states, whether balanced or not, are possible. By moving to a rotating frame, Green *et al.* (2006*a*) carried out a detailed nonlinear investigation in the case of two balls, by computing both isolated branches of periodic solutions and those emanating from Hopf bifurcations of the equilibrium states. Significant regions of bistability were found between these steady and periodic states, chaotic states and states in which the balls rotate at a different angular frequency than the rotor. Furthermore, perturbations were shown to result in a large growth in the vibration before subsequent transient decay. This prompted

the study by Green *et al.* (2006*b*), where the authors used the concept of pseudospectra to analyse this sensitivity to perturbation. It was found there that while the completely balanced state becomes increasingly stable for high rotation frequencies, it also becomes increasingly sensitive to perturbation, with an increasingly larger transient response before settling to the steady state.

Experimental investigations into the use of ADBs can be found in Lee & Van Moorhem (1996), Huang *et al.* (2002) and van de Wouw *et al.* (2005). One of the crucial issues is to design a releasing mechanism for the balancing masses that overcomes a global instability identified in Green (2005), in which the constant speed of the balancing masses lags that of the rotor. This may be partially overcome by clamping the balls in fixed positions until the desired, constant speed of rotation is reached. The balls could then be released at the same speed as the rotor. van de Wouw *et al.* (2005) investigated a different mechanism with many balls in which the energy is dissipated through frictional forces between the balls and the race, which encourages the balls to remain approximately in phase with the rotor. However, a non-zero force is produced when the balls come to rest. Consequently, the steady-state positions are not discrete but instead are found over small ranges of the race. This phenomenon is known as *stiction*. Thus, compared to the viscous damping case, this multiplicity of equilibria is harder to analyse and is more likely to produce a non-zero radial vibration when the balls come to rest.

The aim of this paper is to look at the practical issues associated with an implementation of the ADB on a large-scale rotor. We first consider the effect of using more than two balancing masses. In particular, we show how the stability regions found in Green *et al.* (2006*a*) for the two-ball case change for three and four balls. We have also designed and built an experimental rig inspired by some of the previous experimental results. To overcome some of the observed instabilities, we propose a novel design consisting of a partitioned ball race. However, for our chosen design, we found that the dramatic increase in radial vibration meant that it was not practically possible to break through the first resonance. This setback was also identified in Lee & Van Moorhem (1996). Therefore, in this paper, our experimental investigations will be confined to the case of low rotation speeds.

The rest of the paper is organized as follows. In §2, we recall the equations of motion derived by Green *et al.* (2006*a*) of an eccentric rotor fitted with an ADB consisting of an arbitrary number of balancing balls. From direct analysis of the equations, we identify all possible steady-state solutions, whether balanced or not, and show that the balanced state has a translational degeneracy for more than two balls. Next, in §3 we perform a full nonlinear bifurcation analysis for an ADB with three and four balancing balls, mapping out regions of stable equilibria as parameters in the problem are varied. This is complemented by simulation results obtained by numerical integration. In §4, we introduce the partitioned ball race model and show the results of numerical simulations. In §§5 and 6, we describe our experimental set-up and present results which are compared with numerical simulation results for the corresponding parameter values, where only the experimental viscous damping coefficient has to be identified through fitting. Finally, in §7 we draw conclusions and suggest avenues for future work.

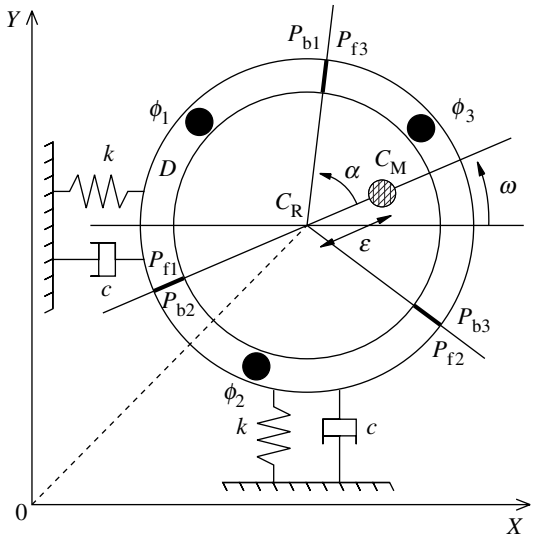

Figure 1. Schematic of an automatic dynamic balancer with a partitioned race (see text for explanation of symbols).

2. Automatic dynamic balancer

An automatic dynamic balancer consists of two or more balancing masses (balls) that are free to move in a ball race that is mounted at a fixed radial distance R from the centre of rotation of a rotor. A rotating disc with an eccentric mass centre, fitted with a partitioned ADB is shown schematically in figure 1 for the case of three balls, where for the time being we shall ignore the presence of the boundaries between partitions $P_{\mathrm{f}i,\mathrm{b}i}$ (i=1, 2, 3).

The race is positioned at a fixed distance from the centre of rotation of the disc and contains a small amount of viscous fluid. The point C_{M} represents the centre of mass of the disc without the balancing masses. It is located at a distance (eccentricity) ε from the centre of rotation C_{R}. The whole rig (rotor plus ADB) is assumed to be isotropically suspended and to rotate at a constant angular velocity ω. For a study into anisotropic support, we refer to Ryzhik *et al.* (2004*b*). Furthermore, all movement is assumed to be constrained to the horizontal (X, Y)-plane, and due to centrifugal forces, the balls are assumed to remain in contact with the race.

(*a*) *Equations of motion*

The equations of motion describing the ADB can be derived using a Lagrangian approach, with generalized coordinates,

$$(X, Y, \phi_1, \phi_2, ..., \phi_n), \tag{2.1}$$

describing the motion of the rotor in the (X, Y)-plane and the angular position of the ith ball, respectively. With the addition of a simple Rayleigh dissipation function representing directly proportional viscous damping in both the ball race

and the rotor suspension system, one obtains

$$M\ddot{X} - M\varepsilon\omega^2 \cos\omega t + \sum_{i=1}^{n} m\{\ddot{X} - R\ddot{\phi}_i \sin(\omega t + \phi_i) - R(\omega + \dot{\phi}_i)^2 \cos(\omega t + \phi_i)\} + kX = -c\dot{X}, \tag{2.2}$$

$$M\ddot{Y} - M\varepsilon\omega^2 \sin\omega t + \sum_{i=1}^{n} m\{\ddot{Y} + R\ddot{\phi}_i \cos(\omega t + \phi_i) - R(\omega + \dot{\phi}_i)^2 \sin(\omega t + \phi_i)\} + kY = -c\dot{Y} \tag{2.3}$$

and

$$-mR[\ddot{X}\sin(\omega t + \phi_i) - \ddot{Y}\cos(\omega t + \phi_i)] + mR^2\ddot{\phi}_i = -D\dot{\phi}_i. \tag{2.4}$$

In this formulation, it is assumed that all balls in the balancer have the same mass m and they all exert the same viscous drag D. The rotor, of mass M and radius R, is assumed to be driven at a constant angular velocity ω and to be isotropically mounted with spring constant k and damping coefficient c. We note that the viscous forces $D\dot{\phi}_i$ acting on the balls have no equal and opposite reaction on the rotor. These viscous forces are insignificant compared with the centripetal forces acting on the rotor due to the balls, and hence are neglected.

(*b*) *Dimensionless form in a rotating frame*

In dimensionless form, the parameters describing the system are: the rotation speed Ω; the external damping ratio ζ; the internal damping β; the mass ratio μ; and the eccentricity δ. These are given as

$$\Omega = \frac{\omega}{\omega_n}, \qquad \zeta = \frac{c}{2\sqrt{kM}}, \qquad \beta = \frac{D}{mR^2\omega_n}, \qquad \mu = \frac{m}{M} \quad \text{and} \quad \delta = \frac{\varepsilon}{R}, \tag{2.5}$$

where ω_n is the natural frequency of the system, given by

$$\omega_n = \sqrt{\frac{k}{M}}. \tag{2.6}$$

We note that, when deriving the following equations of motion, the displacements x and y were rescaled with respect to the radius R, and time rescaled with respect to the natural frequency ω_n.

Our final transformation converts the equations of motion to autonomous equations. We move the frame of reference to the rotating frame using the following substitutions:

$$X = x\cos(\Omega t) - y\sin(\Omega t) \tag{2.7}$$

and

$$Y = x\sin(\Omega t) + y\cos(\Omega t). \tag{2.8}$$

This leads to the following autonomous dynamical system describing the motion of the rotor and ADB in the x and y directions,

$$\begin{pmatrix} 1+n\mu & 0 \\ 0 & 1+n\mu \end{pmatrix}\begin{pmatrix} \ddot{x} \\ \ddot{y} \end{pmatrix} + \begin{pmatrix} 2\zeta & -2\Omega(1+n\mu) \\ 2\Omega(1+n\mu) & 2\zeta \end{pmatrix}\begin{pmatrix} \dot{x} \\ \dot{y} \end{pmatrix} + \begin{pmatrix} K & -2\Omega\zeta \\ 2\Omega\zeta & K \end{pmatrix}\begin{pmatrix} x \\ y \end{pmatrix} = \begin{pmatrix} \delta\Omega^2 \\ 0 \end{pmatrix} + \mu\sum_{i=1}^{n}\begin{pmatrix} (\Omega+\dot{\phi}_i)^2 & \ddot{\phi}_i \\ -\ddot{\phi}_i & (\Omega+\dot{\phi}_i)^2 \end{pmatrix}\begin{pmatrix} \cos\phi_i \\ \sin\phi_i \end{pmatrix} \tag{2.9}$$

and the motion of the ith ball,

$$\ddot{\phi}_i + \beta\dot{\phi}_i - (\ddot{x} - \Omega^2 x - 2\Omega\dot{y})\sin\phi_i + (\ddot{y} - \Omega^2 y + 2\Omega\dot{x})\cos\phi_i = 0, \tag{2.10}$$

where ϕ_i measures the angular position of the ith ball from the line of eccentricity (C_R–C_M in figure 1), $i=1, \ldots, n$. Furthermore, $K = 1 - \Omega^2(1 + n\mu)$ represents the effect of centripetal acceleration. This reduces the effective stiffness of the system and is often called 'spin softening' or 'centripetal softening'. For a full derivation, including the procedure of making these equations dimensionless, we refer to Green *et al.* (2006*a*).

(*c*) *Steady-state analysis*

Green *et al.* (2006*a*) provides a detailed bifurcation analysis of steady states and periodic solutions found in an ADB with two balancing balls. In this paper we consider an ADB with three and four balls showing how this affects the potential stability of the system.

The steady-state solutions are obtained by setting the time derivatives in (2.9) and (2.10) as zero. The steady-state solution can be categorized as balanced when $r = \sqrt{x^2 + y^2} = 0$ or unbalanced when $r = \sqrt{x^2 + y^2} \neq 0$ but the balls come to rest.

A balanced steady state corresponds to the centre of mass of the system being located at the centre of rotation, and satisfies

$$x = y = 0, \quad \sum_{i=1}^{n} \cos\phi_i = -\frac{\delta}{\mu} \quad \text{and} \quad \sum_{i=1}^{n} \sin\phi_i = 0. \tag{2.11}$$

When $n>2$, there exist infinitely many solutions to (2.11). We will refer to these solutions as the sets of balanced state **1**.

As is the case for two balls, unbalanced steady states are found when

$$\frac{y}{x} = \tan\phi_i, \quad i = 1, \ldots, n, \tag{2.12}$$

with solutions

$$\phi_i = \phi_1 + k_i\pi, \quad i = 2, \ldots, n, \; k_i \in \mathbb{Z}. \tag{2.13}$$

Without loss of generality, we consider $k_i=0$ or 1. When $k_i=0$, the first and the ith ball coincide and when $k_i=1$, the first and the ith ball are found on opposite sides of the race to each other, in line with the centre of rotation C_R. We note that in this analysis, collisions between balls are neglected. Physically, this could be realized by considering a multiple ball race (Hwang & Chung 1999).

When all balls coincide ($k_i=0$), solutions, in terms of ϕ_1, are

$$\left.\begin{aligned} x &= \frac{K\Omega^2(n\mu\cos\phi_1 + \delta) + 2n\mu\Omega^3\zeta\sin\phi_1}{K^2 + (2\Omega\zeta)^2} \\ \text{and} \\ y &= \frac{nK\mu\Omega^2\sin\phi_1 - 2\Omega\zeta(\delta\Omega^2 + n\mu\Omega^2\cos\phi_1)}{K^2 + (2\Omega\zeta)^2}, \end{aligned}\right\} \tag{2.14}$$

where

$$\phi_1 = \pm\arccos\left(\frac{-2n\mu\Omega\zeta}{\delta\sqrt{K^2+(2\Omega\zeta)^2}}\right) - \arctan\left(\frac{-K}{2\Omega\zeta}\right), \quad \phi_i = \phi_1,\ i = 2,\ldots,n. \tag{2.15}$$

In what follows, we will refer to (2.14) and (2.15) as the *coincident state* $\mathbf{2}^{\pm}$.

When $(n-m)$ balls lie opposite from m coincident balls ($k_i=1$ for some i), we find solutions

$$\left.\begin{aligned} x &= \frac{K\Omega^2((2m-n)\mu\cos\phi_1+\delta)+2(2m-n)\mu\Omega^3\zeta\sin\phi_1}{K^2+(2\Omega\zeta)^2} \\ \text{and} \\ y &= \frac{(2m-n)K\mu\Omega^2\sin\phi_1-2\Omega\zeta(\delta\Omega^2+(2m-n)\mu\Omega^2\cos\phi_1)}{K^2+(2\Omega\zeta)^2}, \end{aligned}\right\} \tag{2.16}$$

where

$$\phi_1 = \pm\arccos\left(\frac{-2(2m-n)\mu\Omega\zeta}{\delta\sqrt{K^2+(2\Omega\zeta)^2}}\right) - \arctan\left(\frac{-K}{2\Omega\zeta}\right),\ \phi_i = \phi_1, \tag{2.17}$$

$$i = 2,\ldots,m, \quad \phi_j = \phi_1 + \pi,\ j = m+1,\ldots,n.$$

In what follows, we will refer to (2.16) and (2.17) as the $(n-m)$ *in-line states* $\mathbf{3}(\mathbf{n}-\mathbf{m})^{\pm}$.

Again, we refer to Green *et al.* (2006*a*) for an analysis of two balls, i.e. $n=2$ and consequently, in (2.16) and (2.17), $m=1$. Here we consider three and four balancing balls.

For $n=3$, we can either have $m=1$ or 2. However, as the balls are identical so are these states, i.e. at any one time we have one separate and two coincident balls. The sign of (2.17) determines the region where the separate (or the coincident) ball(s) are with respect to the imbalance. Hence we refer to the in-line states, with three balls, simply as $\mathbf{3}^{\pm}$.

For $n=4$, we have three situations, one where two balls are coincident ($m=2$) and one where three balls are coincident ($m=3$). (The latter state being identical to $m=1$.) We will refer to these four-ball, in-line states as **3A** and $\mathbf{3B}^{\pm}$, respectively.

(*d*) *Conditions for existence of steady states*

Analogous to the two-ball case, (2.11) implies that, for a balanced state **1** to exist,

$$\mu \geq \mu_c := \frac{\delta}{n}. \tag{2.18}$$

In other words, to achieve balance, the combined mass of the balls must be large enough to cope with the eccentricity δ. Note that when equality is reached, this corresponds to the coincident states $\mathbf{2}^{\pm}$.

The coincident states $\mathbf{2}^{\pm}$ exist only if the modulus of the argument of the inverse cosine of (2.15) is less than unity, i.e.

$$K^2 > (2\Omega\zeta)^2\left(\left(\frac{n\mu}{\delta}\right)^2 - 1\right). \tag{2.19}$$

As for the two-ball case, when $\mu < \mu_c$, the states $\mathbf{2}^{\pm}$ always exist.

Likewise, from (2.17), the in-line states $\mathbf{3}(\mathbf{n}-\mathbf{m})^{\pm}$ exist if

$$K^2 > (2\Omega\zeta)^2\left(\left(\frac{(2m-n)\mu}{\delta}\right)^2 - 1\right). \tag{2.20}$$

In other words, they exist for $\mu < \delta(2m-n)$.

The existence of the coincident and the in-line states, above the critical values of μ, depends on the other parameters δ, ζ and β in a non-trivial way. To investigate this, we turn to numerical bifurcation techniques.

3. Numerical results for multiple balls

In this section we investigate the stability of the steady states identified in §2*c* using numerical bifurcation techniques. Namely, we compute the boundaries between solutions with differing stability using the continuation package MATCONT (Dhooge *et al.* 2004). In this way, a detailed map is produced showing how regions of stability change as parameters are varied. These results will be backed up by direct simulation of the equations of motion.

In each case, where appropriate, the fixed parameters are given as

$$\beta = \delta = \zeta = 0.01 \quad \text{and} \quad \mu = 0.05. \tag{3.1}$$

These parameters were chosen to allow direct comparison with the two-ball ADB study of Green *et al.* (2006*a*).

(*a*) *Steady-state bifurcation diagram for n=3*

We start by investigating the ADB with three balancing balls. Figure 2*a–d* shows two-parameter bifurcation diagrams for Ω versus μ, δ, ζ and β, respectively. The dark shaded regions of figure 2 indicate regions of parameter space in which the balanced state **1** is stable. The lighter shaded regions correspond to parameters at which one of the coincident states $\mathbf{2}^{\pm}$ is stable. The unshaded regions correspond to regions of instability. Solid lines correspond to bifurcations of states **1** and $\mathbf{2}^{\pm}$, while dashed lines correspond to bifurcations of states $\mathbf{3}^{\pm}$. The curves are labelled as Hopf bifurcations 'H' (oscillatory instabilities) which occur when a pair of pure imaginary eigenvalues cross the imaginary axis and saddle-node bifurcations 'SN' (steady-state instabilities), which due to symmetry are actually pitchfork bifurcations for some of the states. In the latter case, a real eigenvalue crosses the imaginary axis (Kuznetsov 1997). Furthermore, as there are infinitely many balanced states, we fix $\phi_3 = \pi$ when analysing the bifurcations of state **1**. This is equivalent to computing bifurcations of state **1** for the two-ball case with a different δ to that used by Green *et al.* (2006*a*). Likewise, the coincident states may be compared to a two-ball case where the masses of the balls are increased, and the in-line states to the case where each ball has a different mass.

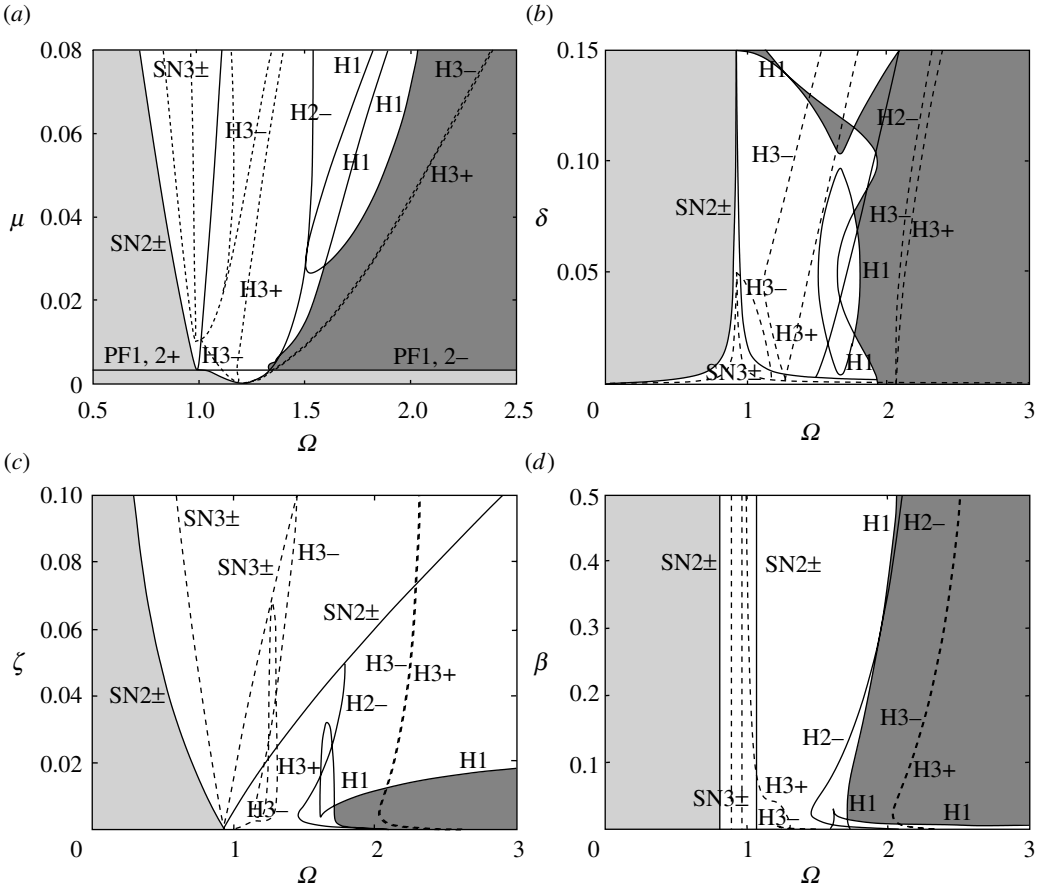

Figure 2. Two-parameter bifurcation diagrams of steady-state solutions in the three-ball ADB. (Solid lines, saddle-node bifurcations SN and Hopf bifurcations H of states **1** and $\mathbf{2}\pm$; broken lines, bifurcations of state **3**; dark shaded regions, stable state **1**; lighter shaded regions, stable state $\mathbf{2}^-$.) When fixed, the parameters are $\beta=\delta=\zeta=0.01$ and $\mu=0.05$. The varying parameters are (*a*) Ω versus μ, (*b*) Ω versus δ, (*c*) Ω versus ξ and (*d*) Ω versus β.

It is clear from these bifurcation diagrams that for low rotation speeds the coincident states $\mathbf{2}^{\pm}$ are stable. Specifically, it can be shown that this is state $\mathbf{2}^-$. While for high rotation speeds the balanced state **1** is shown to be stable. Furthermore, figure 2*b* shows a region of stability, for high eccentricity δ, of the balanced state **1**, close to the resonant rotation speed $\Omega=1$. This is our first indication that the addition of more balancing balls changes the stability properties. We recall that in Green *et al.* (2006*a*), the two-ball ADB was shown to exhibit a small region of stability close to this resonant speed in all parameter planes. Moreover, it was shown that this small region of stability was accessible only through a very limited range of initial conditions. In other words, for intermediate rotation speeds, and random initial conditions, the system is likely to be drawn into unstable, possibly chaotic dynamics. However, the three-ball ADB shows less stability close to the resonant speed, for the parameter range under consideration. Finally, in the (Ω, μ)-plane and for low values of μ, the coincident states $\mathbf{2}^{\pm}$ are stable. Again, it can be shown that this is state $\mathbf{2}^-$.

Moreover, for each of the parameter sets under consideration, and starting within a region of balanced equilibrium (dark shading), the following scenario holds: for decreasing Ω, the balanced state **1** is destabilized in a Hopf bifurcation H1. The dynamics then enter a region of non-steady-state behaviour, containing periodic oscillations through to chaotic motion. Decreasing Ω further sees a saddle-node bifurcation SN2$\pm$. At this point, the two coincident states $\mathbf{2}^{\pm}$ are born. Again, we have that the state $\mathbf{2}^{-}$ is stable, while the state $\mathbf{2}^{+}$ is unstable.

Figure 2*c* shows that the region of stability of the balanced state **1** in the (Ω, δ)-plane is small. This is again in stark contrast with the two-ball case, in which this region of stability was seen to cover approximately half of the parameter plane under consideration. This shows that increasing the number of balancing masses has a detrimental effect on whether or not stability can be achieved for the range of parameters under consideration. Physically, this implies that the three-ball ADB cannot achieve balance when the rotor damping ζ is too high. We note that the bifurcation diagram in the (Ω, β)-plane is practically identical to the two-ball case.

Like the two-ball case, the states $\mathbf{3}^{\pm}$ were found to be always unstable. However, it is involved in an interesting bifurcation scenario. Figure 3*a–c* shows one-parameter bifurcation diagrams, for the three-ball ADB, for $\mu=0.05$, 0.005 and 0.0025, respectively, i.e. for an increasing rotor mass to ball mass ratio. For large μ, figure 3*a* shows that the four states $\mathbf{2}^{\pm}$ and $\mathbf{3}^{\pm}$ are born in two separate saddle-node bifurcations. These occur at the left and right edges of the 'v'-shaped curves SN2$\pm$ and SN3$\pm$, as shown in figure 2*a*. Decreasing μ sees one pass the base of the 'v' representing the saddle-node curve SN3$\pm$ while still inside the v-shaped curve SN2$\pm$ (figure 2*a*). Figure 3*b* shows a one-parameter transition at such a value of μ, namely $\mu=0.005$. It is clear that the two sets of states $\mathbf{2}^{\pm}$ are still born in two separate saddle-node bifurcations SN2$\pm$. However, the two sets of states $\mathbf{3}^{\pm}$ have now merged into two curves; a lower curve on which one finds the state $\mathbf{3}^{+}$ and an upper curve on which one finds the state $\mathbf{3}^{-}$. The states $\mathbf{3}^{\pm}$ now exist for all Ω. Finally, figure 3*c* shows that by decreasing μ further to $\mu=0.0025$ we pass the base of the 'v' representing the saddle-node curve SN2$\pm$ (again see figure 2*a*). Similar to the case for the states $\mathbf{3}^{\pm}$, the sets of states $\mathbf{2}^{\pm}$ merge together. They form an upper curve consisting of state $\mathbf{2}^{-}$ and a lower curve consisting of state $\mathbf{2}^{+}$. Subsequently, for low values of μ, both the states $\mathbf{2}^{\pm}$ and $\mathbf{3}^{\pm}$ exist for all Ω.

(*b*) *Steady-state bifurcation diagram for* $n=4$

Figure 4*a–d* shows two-parameter bifurcation diagrams for the four-ball ADB. The notation used is the same as for the three-ball diagrams of figure 2. The exception being that the in-line state **3** now comes in two varieties: **3A** and $\mathbf{3B}^{\pm}$ (recall §2*c*). Again, as there are infinitely many balanced states **1**, we fix $\phi_3=\pi$ and $\phi_4=-\pi$ when computing bifurcations of state **1**. Once more, the balanced state **1** is shown to be stable for high rotation speeds, while the coincident state $\mathbf{2}^{-}$ is stable for low rotation speeds or low mass ratios μ. Interestingly, however, the region of stability around the resonant speed ($\Omega=1$), identified for the two-ball ADB in Green *et al.* (2006*a*) but shown to disappear for the three-ball ADB in figure 2*a*, reappears for the four-ball ADB. In fact, figure 4*b* shows that this region of stability now occurs for both low and high values of δ. It is clearly seen that all regions of stability of state **1** are connected to the Hopf curve H1. (In fact, the regions of stability of state **1** are connected by this curve for large values of μ in figure 4*a–d*.)

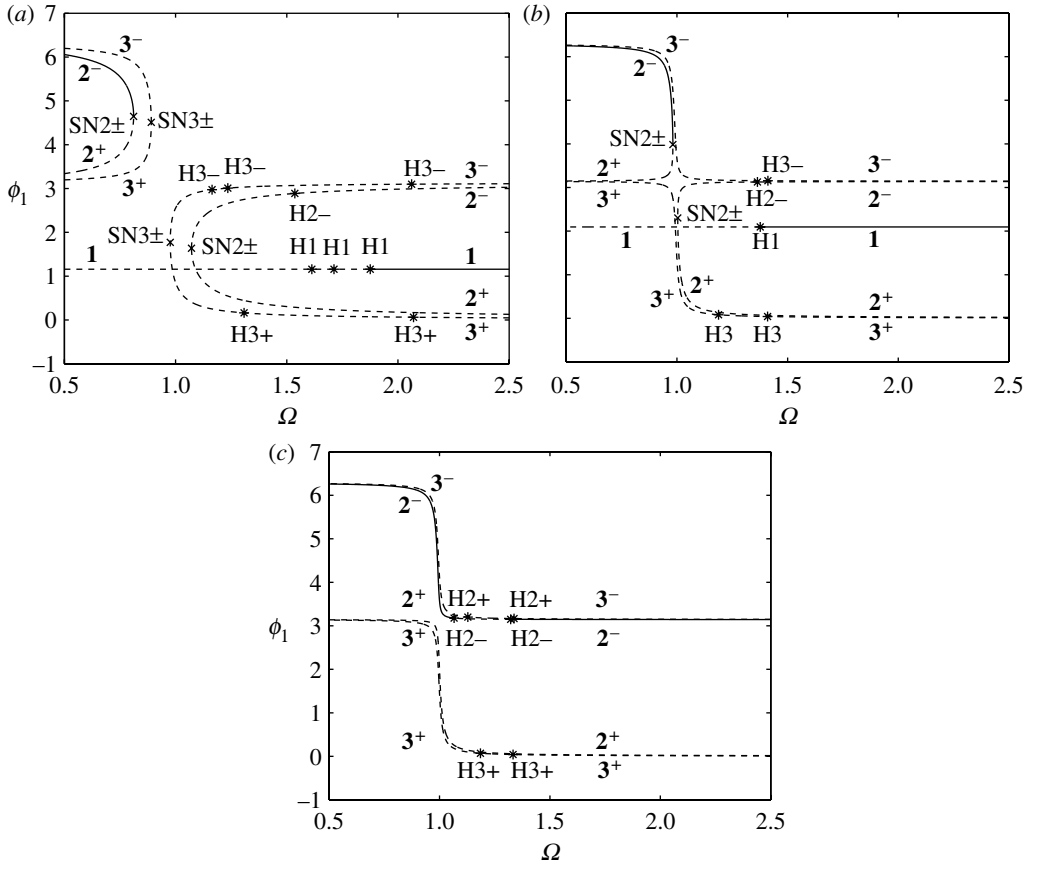

Figure 3. One-parameter bifurcation diagrams for the three-ball ADB. Diagrams for Ω versus ϕ_1 for (*a*) $\mu=0.05$, (*b*) $\mu=0.005$ and (*c*) $\mu=0.0025$. (Solid lines, stable states; broken lines, unstable states; the numbers indicating the type of state). Saddle-node bifurcations are denoted by crosses and Hopf bifurcations by asterisks.

Figure 4*c* shows that upon increasing the number of balls, the region of stability of state **1** in the (Ω, δ)-plane shrinks further. Moreover, the region of stable operation of state $\mathbf{2}^-$, for low rotation speeds, is also shown to decrease in size. The unshaded region of instability is shown to dominate the (Ω, δ)-plane. Finally, again, figure 4*d* shows little quantitative change in the stability structure of the (Ω, β)-plane. However, the large region of stability of state **1** does move further to the right. In other words, increasing the number of balls is again shown to increase the size of the region of instability.

We note that the states **3A** and $\mathbf{3B}^{\pm}$ are always unstable. The interesting bifurcation scenario outlined in figure 3 occurs again for the four-ball ADB.

(*c*) *Numerical simulation results*

We now present results obtained by numerical integration of the system (2.9) and (2.10). We restrict ourselves to the case of three balls only, in order to illustrate the extra complexity of having degenerated equilibria when $n>2$. Our aim is merely to show the different steady states identified in §2. A complete

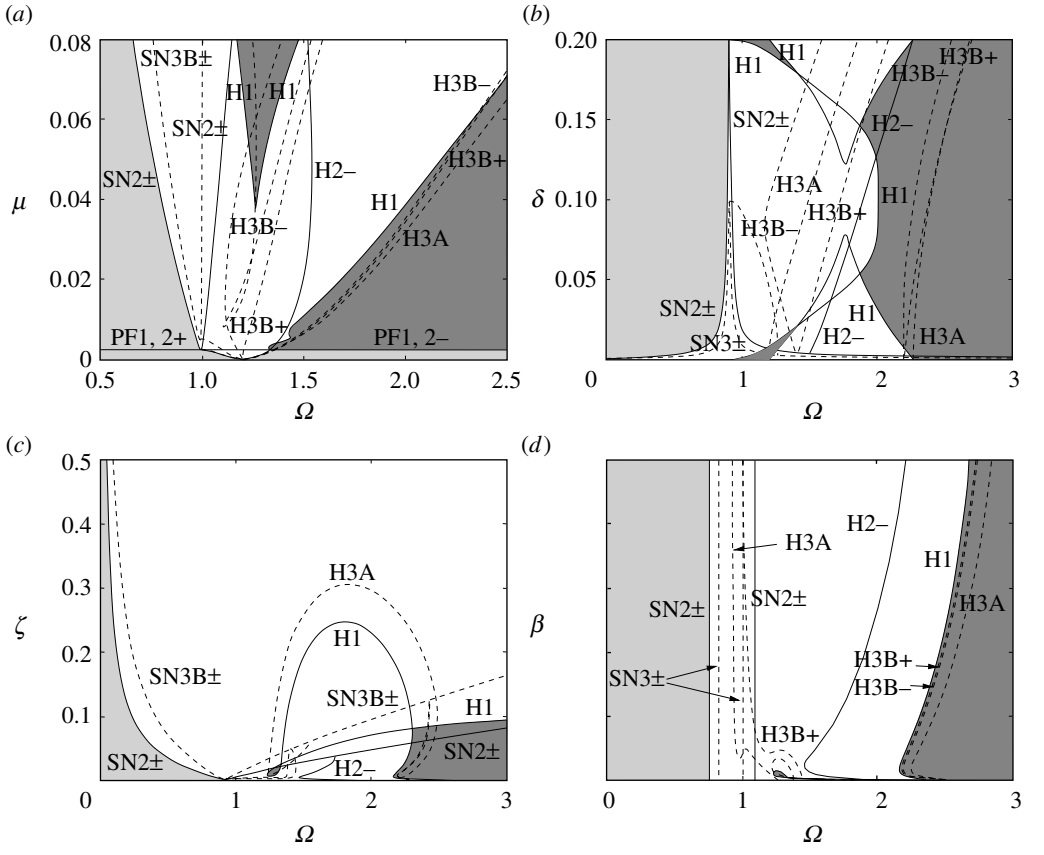

Figure 4. Bifurcation diagrams of steady-state solutions in the four-ball ADB. (Solid lines, saddle-node bifurcations SN and Hopf bifurcations H of states **1** and **2**±; broken lines, bifurcations of state 3; dark shaded regions, stable state **1**; lighter shaded regions, stable state $\mathbf{2}^{-}$.) When fixed, the parameters are $\beta=\delta=\zeta=0.01$ and $\mu=0.05$. The varying parameters are (*a*) Ω versus μ, (*b*) Ω versus δ, (*c*) Ω versus ξ and (*d*) Ω versus β.

transient analysis, including multistability between steady states and possible periodic states, emanating from the Hopf bifurcations identified above, is beyond the scope of this study.

Figure 5 shows the time evolution of the radial vibration $r=\sqrt{x^2+y^2}$ (figure 5*a*) and the angular position of each of the three balancing balls $\phi_{1,2,3}$ (figure 5*b*). Initial conditions were taken such that one ball was launched directly opposite to the imbalance, with the other two launched from symmetric positions at an angular distance of $\pi/3$ from the imbalance, namely $\phi_1(0)=\pi/3$, $\phi_2(0)=\pi$ and $\phi_3(0)=5\pi/3$. Note that if the balls were clamped in this way during an acceleration phase, they would not add to the imbalance. Parameters were fixed at $\Omega=2.5$, $\zeta=0.01$, $\beta=0.01$, $\delta=0.01$ and $\mu=0.05$. As identified in figure 2 the radial vibration is seen to reduce to zero. In other words, the ADB has balanced the eccentric rotor.

Figure 6 shows the time evolution of r and $\phi_{1,2,3}$ for $\Omega=0.5$, $\zeta=0.01$, $\beta=0.01$, $\delta=0.01$ and $\mu=0.05$. Again the balls were initially fixed at $\phi_1(0)=\pi/3$, $\phi_2(0)=\pi$ and $\phi_3(0)=5\pi/3$. It is clearly seen that, for these parameters, the balls converge to the same angular position. This is the coincident state predicted in figure 2.

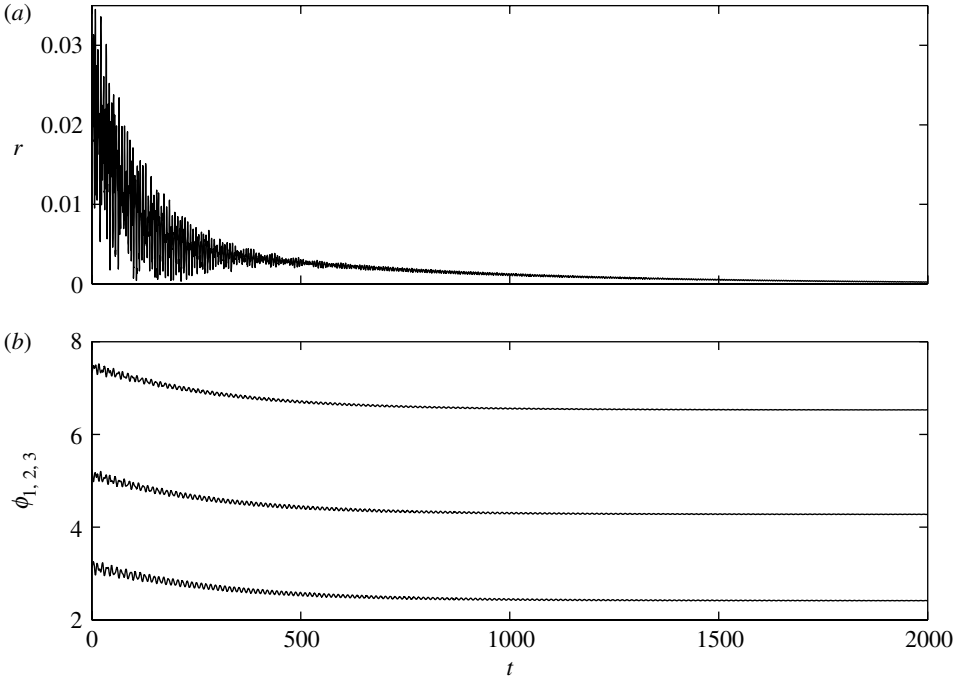

Figure 5. Time evolution of an ADB with three balls for $\Omega=2.5$. Other parameters were fixed at $\zeta=0.01$, $\beta=0.01$, $\delta=0.01$ and $\mu=0.05$. (*a*) The radial vibration $r=\sqrt{x^2+y^2}$ and (*b*) the ball positions $\phi_{1,2,3}$ against time t. Initial conditions were fixed at $x=y=\dot{x}=\dot{y}=0$, $\dot{\phi}_1=\dot{\phi}_2=\dot{\phi}_3=0$, $\phi_1=\pi/3$, $\phi_2=\pi$ and $\phi_3=5\pi/3$.

Finally, figure 7 shows the dynamics for $\Omega=1.6$. All other parameters and initial conditions remain unchanged. For this value of Ω, figure 2 predicts no stable dynamics. This is clearly seen in figure 7. The radial vibration r exhibits chaotic dynamics (figure 7*a*), while the angular position of each ball is seen to continually decrease; a constant rotation modulo 2π (figure 7*b*). The speed of the imbalance has exceeded the average speed of each ball. In fact, as well as reaching a speed which lags that of the rotor, the positions of the balls are also undergoing chaotic motion. This is akin to the instability identified in Green (2005). We note that with two or more balls, one or more may undergo this instability while the rest maintain pace with the speed of the rotor (see fig. 9(d) of Green *et al.* (2006*a*)).

(*d*) *Discussion on optimal number of balls*

The results obtained so far suggest that there is little advantage in increasing the number of balls in the ADB, purely in terms of the size of the parameter region in which the balanced state **1** is stable. For rotors whose rotation speeds are sufficiently beyond the fundamental resonance $\Omega=1$, this issue is not so crucial and it is more important to assess the sensitivity of the balanced state to perturbations, and the size of its basin of attraction. Without repeating the detailed analysis by Green *et al.* (2006*b*), this aspect of the problem is not so clear for more balls, but preliminary computations suggest that the problem is more

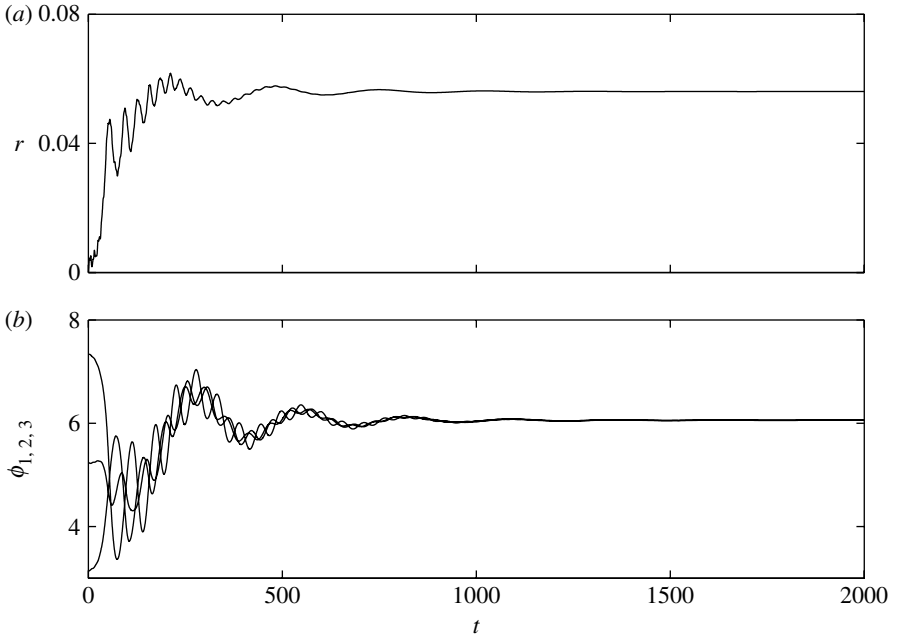

Figure 6. Time evolution of an ADB with three balls $\Omega=0.5$. Other parameters were fixed at $\zeta=0.01$, $\beta=0.01$, $\delta=0.01$ and $\mu=0.05$. (*a*) The radial vibration $r=\sqrt{x^2+y^2}$ and (*b*) the ball positions $\phi_{1,2,3}$ against time t. Initial conditions were fixed at $x=y=\dot{x}=\dot{y}=0$, $\dot{\phi}_1=\dot{\phi}_2=\dot{\phi}_3=0$, $\phi_1=\pi/3$, $\phi_2=\pi$ and $\phi_3=5\pi/3$.

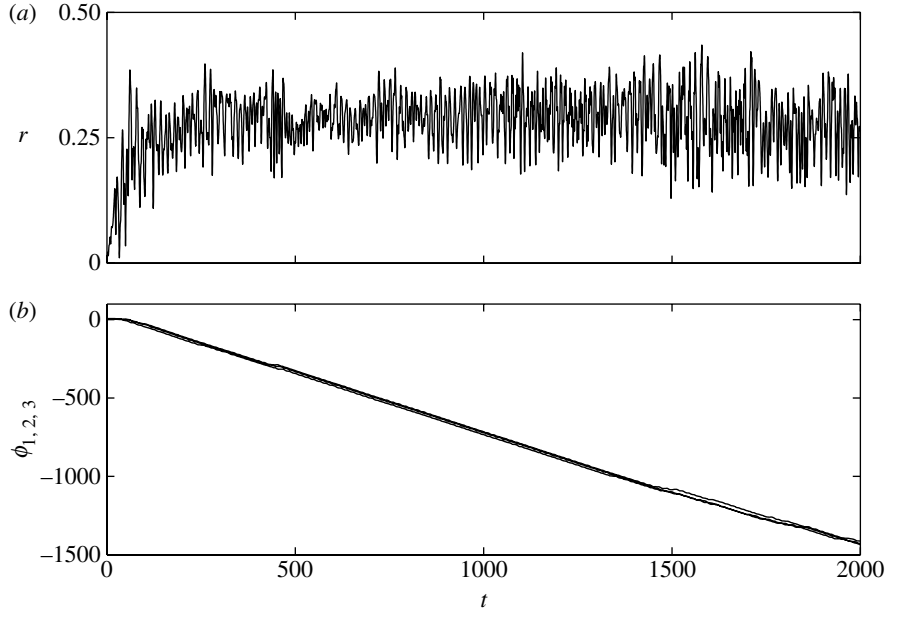

Figure 7. Time evolution of an ADB with three balls for $\Omega=1.6$. Other parameters were fixed at $\zeta=0.01$, $\beta=0.01$, $\delta=0.01$ and $\mu=0.05$. (*a*) The radial vibration $r=\sqrt{x^2+y^2}$ and (*b*) the ball positions $\phi_{1,2,3}$ against time t. Initial conditions were fixed at $x=y=\dot{x}=\dot{y}=0$, $\dot{\phi}_1=\dot{\phi}_2=\dot{\phi}_3=0$, $\phi_1=\pi/3$, $\phi_2=\pi$ and $\phi_3=5\pi/3$.

robust, i.e. the basin of attraction is larger, for high rotation speeds with an increased number of balls. Thus, at this stage, there is no general conclusion possible on the optimum number of balls and the choice would depend on the specific details of the implementation of the ABD.

4. Partitioned ball race

Once the dynamics converge to the rotating state identified in figure 7, one cannot attain stability for higher rotation speeds simply by ramping up the speed. This instability may easily be reached through an acceleration phase, as identified by Green (2005), i.e. by increasing the rotation frequency through the resonant speed, which causes the balls to slip and thus have a speed less than that of the rotor. One solution to this problem would be to clamp the balls in fixed positions until the desired, constant speed of rotation is reached (Ernst 1951). The balls could then be released at the same speed as the rotor. Another solution, which we introduce here for the first time, is to place partitions in the ball race, dividing the race into *sectors* of equal arc-length, with one ball in each partition. During a rapid acceleration phase, the balls would be forced to rest against their lagging partition. After the acceleration, the balls would have the same speed as the rotor (from an external observer's point of view).

Intuitively, in order to achieve a balanced state it would seem necessary to have at least three partitions. In the case of two balls, there is no degeneracy (internal degree of freedom) in the balanced equilibrium state. Hence, for certain positions of imbalance, the fixed partitions will not allow the balls to migrate to this equilibrium position. For three or more balls, we have an internal degree of freedom that allows balance to be achieved (at appropriate parameter values for which the state **1** exists) no matter where the partitions are placed with respect to the imbalance. Hence, in what follows we shall consider the case of three partitions exclusively.

A partitioned ball race has other potential advantages. Firstly, the coincident equilibrium state is not possible. This equilibrium results in an increased imbalance when it is stable, which is general for subcritical rotation speeds. The elimination of this state might lead to more favourable subcritical behaviour. Another advantage is that collisions between balls (an effect we have not included in our model) cannot occur. Instead, we have collision between balls and partitions only, which can be designed to have specific desired properties leading to impacting behaviour with either high or low coefficients of restitution.

Figure 1 shows a schematic of an ADB with such a partitioned race with three partitions $P_{\mathrm{f}i,\mathrm{b}i}$ ($i=1, 2, 3$). Here subscript b denotes the back (lagging) face and f the front (leading) face of a partition with respect to the direction of rotation. The equations of motion governing this system are the same as (2.9) and (2.10), together with the following impact law, modelling the collisions of the balls with their respective partitions:

$$\left.\begin{aligned} &\text{if} \quad \phi_i = \alpha + \frac{2(i-1)\pi}{n} + r_{\mathrm{b}} \quad \text{or} \quad \phi_i = \alpha + \frac{2i\pi}{n} - r_{\mathrm{b}}, \\ &\text{then} \quad \dot{\phi}_i \to -e\dot{\phi}_i, \quad e \in [0,1], \quad i = 1, \ldots, n. \end{aligned}\right\} \tag{4.1}$$

Additional parameters include r_{b}, the angular diameter of the ball; α, the angle to the first partition from the line of imbalance (C_{R} to C_{M}); and a coefficient of

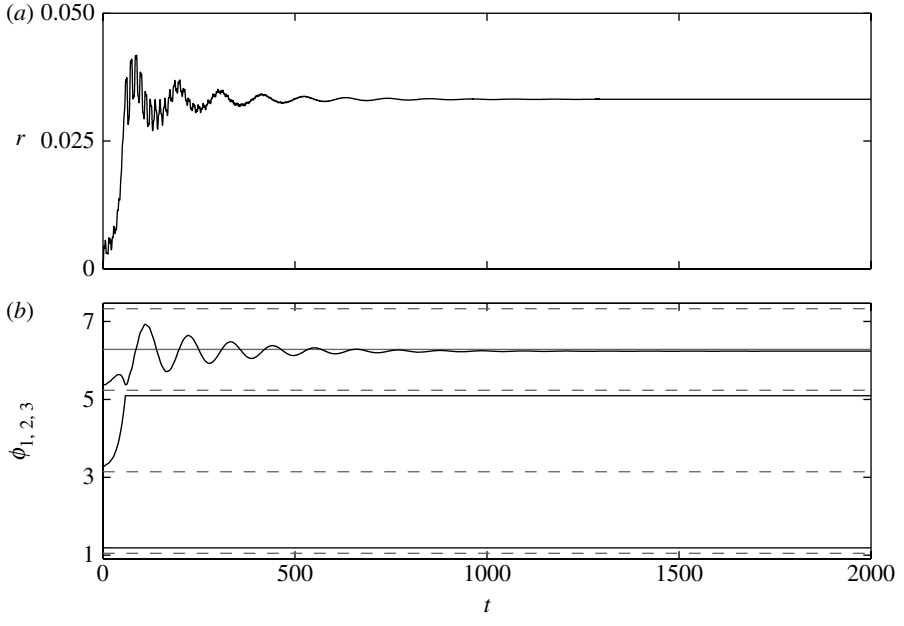

Figure 8. Time evolution of a partitioned ADB with three balls for $\Omega=0.5$. Other parameters were fixed at $\zeta=0.01$, $\beta=0.01$, $\delta=0.01$ and $\mu=0.05$. (*a*) The radial vibration $r=\sqrt{x^2+y^2}$ and (*b*) the ball positions $\phi_{1,2,3}$ against time t. Initial conditions were fixed at $x=y=\dot{x}=\dot{y}=0$, $\dot{\phi}_1=\dot{\phi}_2=\dot{\phi}_3=0$, $\phi_1=\pi/3+r_\mathrm{b}$, $\phi_2=\pi+r_\mathrm{b}$ and $\phi_3=5\pi/3+r_\mathrm{b}$.

restitution e. In other words, this law states that when a ball impacts with its partition, its direction of motion is reversed and its speed is multiplied by e.

To show that the dynamics are consistent with those identified in §3*c*, figure 8 shows the evolution of the radial vibration $r=\sqrt{x^2+y^2}$ (figure 8*a*) and the angular positions of the balls (figure 8*b*) for $\Omega=0.5$. After an acceleration phase, the initial conditions of the balls were fixed at $\phi_1(0)=\pi/3+r_\mathrm{b}$, $\phi_2(0)=\pi+r_\mathrm{b}$ and $\phi_3(0)=5\pi/3+r_\mathrm{b}$; $r_\mathrm{b}=0.14$. Parameters were fixed to coincide with those used in §3*c*, namely $\zeta=0.01$, $\beta=0.01$, $\delta=0.01$ and $\mu=0.05$. Additional parameters were fixed at $\alpha=\pi/3$ and $e=0.001$. This small value of e was chosen to model the impact between the ball and the grub screw; the actual contact taking place near the top of the ball. In figure 8*b*, the partitions are marked by grey dashed lines and the position of the imbalance by a solid (grey) line (at $\phi_\mathrm{i}=2\pi$). For this low rotation speed, it is clear that the balls want to move to the coincident states $\mathbf{2}^{\pm}$ identified in figure 6. However, the partitions impede their progress. As expected, this results in a lower radial vibration of $r\approx0.032$ when compared with $r\approx0.056$ (recall figure 6*a*).

Figure 9 shows the dynamics for $\Omega=1.6$. At this rotation speed, figure 7 identified the instability in which the speed of the balls lags that of the rotor. The partitions obviously stop such dynamics. Instead, the balls continuously impact between their leading and lagging partitions in a periodic manner. However, this bouncing motion has an alarming effect on the radial vibration, which increases above $r=1$.

Finally, figure 10 shows the dynamics for $\Omega=2.5$. The system is clearly seen to balance; the radial vibration r goes to zero, while, after one impact with their respective leading partitions, the balls come to rest away from their partitions.

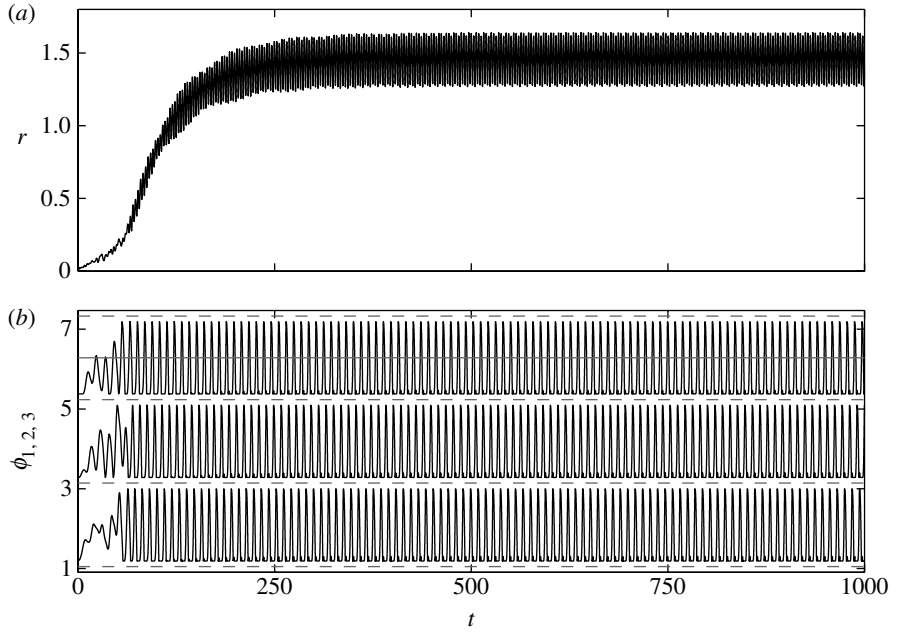

Figure 9. Time evolution of a partitioned ADB with three balls for $\Omega=1.6$. Other parameters were fixed at $\zeta=0.01$, $\beta=0.01$, $\delta=0.01$ and $\mu=0.05$. (*a*) The radial vibration $r=\sqrt{x^2+y^2}$ and (*b*) the ball positions $\phi_{1,2,3}$ against time t. Initial conditions were fixed at $x=y=\dot{x}=\dot{y}=0$, $\dot{\phi}_1=\dot{\phi}_2=\dot{\phi}_3=0$, $\phi_1=\pi/3+r_\mathrm{b}$, $\phi_2=\pi+r_\mathrm{b}$ and $\phi_3=5\pi/3+r_\mathrm{b}$.

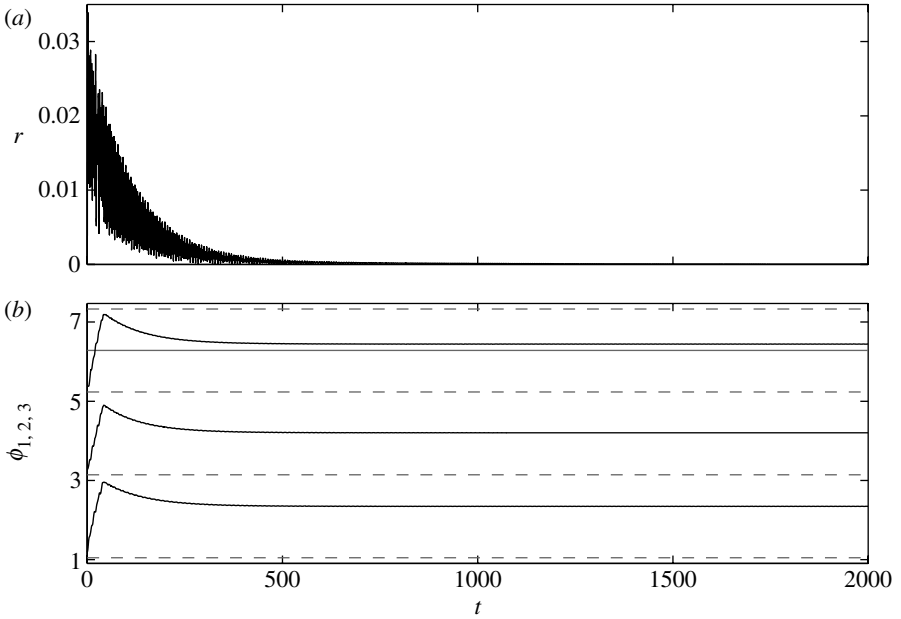

Figure 10. Time evolution of a partitioned ADB with three balls for $\Omega=2.5$. Other parameters were fixed at $\zeta=0.01$, $\beta=0.01$, $\delta=0.01$ and $\mu=0.05$. (*a*) The radial vibration $r=\sqrt{x^2+y^2}$ and (*b*) the ball positions $\phi_{1,2,3}$ against time t. Initial conditions were fixed at $x=y=\dot{x}=\dot{y}=0$, $\dot{\phi}_1=\dot{\phi}_2=\dot{\phi}_3=0$, $\phi_1=\pi/3+r_\mathrm{b}$, $\phi_2=\pi+r_\mathrm{b}$ and $\phi_3=5\pi/3+r_\mathrm{b}$.

Interestingly, the time it takes for the ADB to balance the rotor is far shorter than for the unpartitioned case (compare with figure 5).

5. Experimental results

In an attempt to verify our numerical results, we designed and built an eccentric rotor fitted with an ADB (figure 11). This consisted of an aluminium rotor hub with a radius of 155 mm into which a steel ball race centred at a radial distance of 105 mm was machined. The total mass of the hub was 10 kg. Steel balls with 30 mm diameter, 0.110 g mass were used as balancing masses. These balls were visible through a perspex covering, into which grub screws were sunk in order to form the partitions. An imbalance was added by attaching bolts to the extremity of the hub. The rotor was fitted midway along a silver steel shaft of 30 mm diameter. The effective length of the shaft could be varied by moving bearing supports situated above and below the rotor. The whole set-up was mounted vertically (so that gravitational effects could be neglected) and was driven by a variable speed DC motor, through a flexible coupling, fitted above the shaft.

In the results presented here, a 100 g bolt was used as an imbalance. The bearing supports were fitted to provide an effective shaft length of 1.305 m. Furthermore, the ball race was coated with a thin layer of hydraulic fluid to provide some resistance to the movement of the balls against the race.

At rest, a modal analysis was performed using LMS Test Lab software to estimate the first resonance of the entire system. This was found to be $\omega_n = 29.5$ Hz. Using this first resonance, a half-power bandwidth method gave the external damping coefficient of the system as $c = 0.052\ \mathrm{N\,s\,m^{-1}}$, while the spring coefficient of the shaft and rotor system was calculated as $k = 3.436 \times 10^5\ \mathrm{N\,m^{-1}}$. During rotation, a Polytec Doppler laser vibrometer was used to measure the vibration of the rotor and record the vibration spectra. Furthermore, a strobe light (figure 11) and a video camera were used to visualize and record the ball positions. The speed of the rotor and the frequency of the strobe light were controlled using dSpace software.

(a) *Steady-state ball configurations*

During our experimental investigations, in addition to the situation in which the balls were *fixed* in a symmetric configuration, so as to not add to the imbalance, we identified two further coexisting configurations in which the balls came to rest in the ADB.

Figure 12 shows these two configurations for a frequency of 10 Hz ($\Omega = 0.339$). The partitions are highlighted by diamonds and the imbalance by a square. The positions of the balls are highlighted by large dots.

Figure 12*a* shows the first configuration, which we will refer to as *free*. Here the ball closest to the imbalance moves furthest from its lagging partition P_{3b}. While the other two balls both move away from their lagging partitions; the ball directly opposite to the imbalance moves furthest. Both balls come to rest in the ball race. This free-ball configuration was seen to be stable up to a rotation frequency of approximately 11.5 Hz ($\Omega = 0.390$). Furthermore, it was shown to be robust against external perturbation, namely striking of the shaft or the underside of the rotor.

For frequencies above approximately 11.5 Hz, the free-ball configuration was destabilized. The resulting position of the balls is shown in figure 12*b*. It is clear

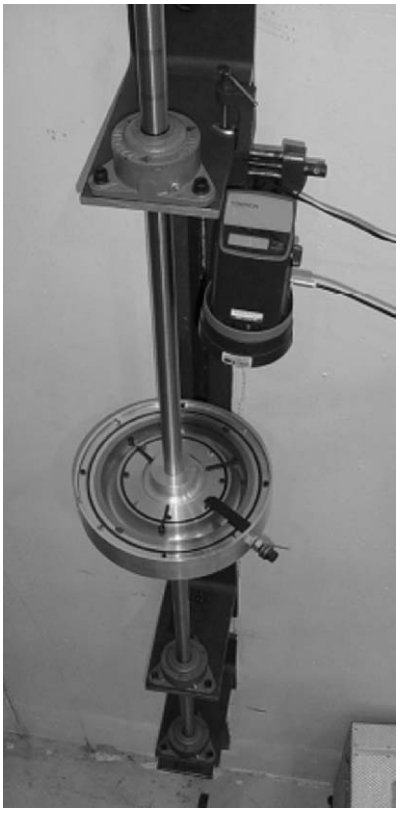

Figure 11. Experimental rig.

that the balls move as far as possible towards the imbalance, as would be expected for subcritical rotation speeds. This results in the ball closest to the imbalance coming to rest between the lower two partitions of figure 12, with the other two balls coming to rest against these two partitions. This configuration is analogous to the coincident steady states $\mathbf{2}^{\pm}$ identified in §2*c* and shown in figure 8. Hence, we will refer to this as the *coincident*-ball configuration.

(*b*) *Experimental bifurcation diagrams*

Figure 13 shows the result of our experimental investigations. The average displacement, taken from the maximum of the first peak of the vibration spectra, averaged over nine runs, is shown versus the rotation frequency. This peak corresponds to the speed of rotation, also known as the 'synchronous response'. The circles correspond to measurements in which the balls were fixed; the squares correspond to measurements in which the balls were free (figure 12*a*); and the crosses correspond to measurements after the free configuration destabilized resulting in the coincident configuration (figure 12*b*).

Quantitative similarities exist between each experimental run. Namely, for the lowest frequencies considered, the free-ball configuration resulted in the least vibration, followed by the coincident and fixed configurations. By increasing the frequency of

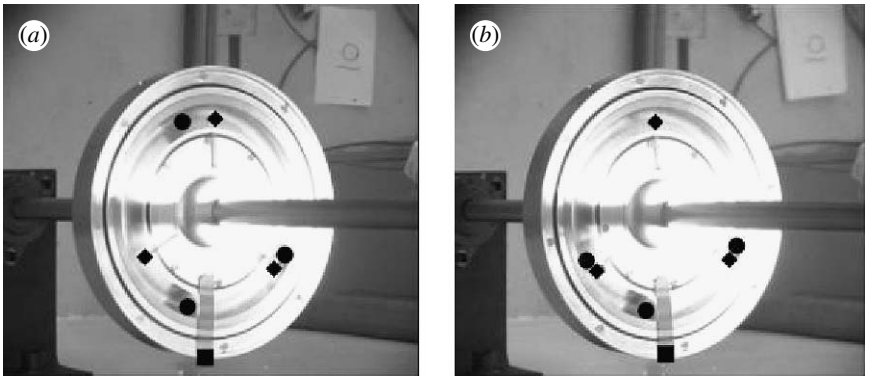

Figure 12. Steady-state ball configurations. Three-ball steady-state configurations: (*a*) free and (*b*) coincident. The dots highlight the position of the balls; the diamonds, the position of the partitions; and the square, the position of the imbalance. Rotation is in the anticlockwise direction.

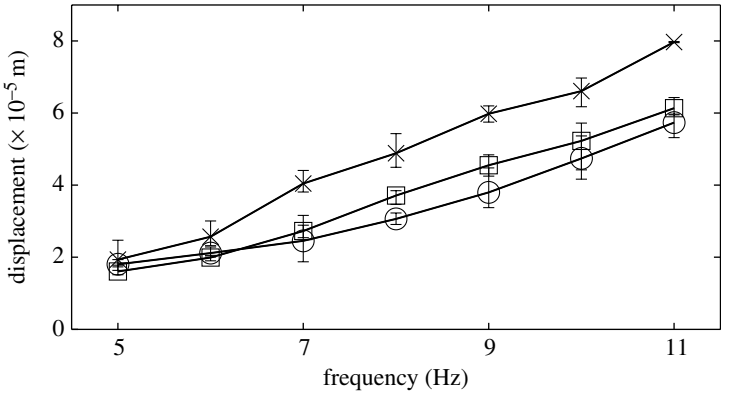

Figure 13. Synchronous response versus speed of rotation. Maxima of the first peak of the averaged vibration spectra showing fixed-ball positions (circles), free-ball positions (squares) and coincident-ball positions (crosses). The ends of the error bars correspond to the maximum and minimum deviations from the mean measurements.

rotation, interestingly, the free-ball configuration continues to result in a lower vibration than the fixed-ball configuration for a short range of frequencies. However, the fixed-ball configuration is eventually shown to result in the least vibration for higher frequencies. The free-ball configuration is still stable at these higher frequencies, finally becoming unstable at approximately 11.5 Hz ($\Omega = 0.390$). The balls move to the coincident configuration after this instability. As expected, the coincident configuration results in the greatest vibration at all frequencies.

6. Numerical bifurcation diagrams

We now compare the experimental results with those obtained using numerical techniques. Namely, we numerically integrate equations (2.9), (2.10) and (4.1), computing bifurcation diagrams for increasing Ω. Parameters were chosen to

correspond to the experiment, namely $\delta=0.0148$, $\mu=0.011$, $\zeta=1.4027\times10^{-5}$, $r_b=0.14$ and $e=0.001$. Furthermore, as β is an uncertain quantity, we perform this analysis for different values of β.

Figure 14*a–c* shows numerical results computed with MATLAB for $\beta=0.1$, 0.3 and 1.0, respectively. Event detection routines were used to model the collisions of the balls with the partitions. After a long initial transient period of $t=10\ 000$, the extrema of the radial vibration $r=\sqrt{x^2+y^2}$ have been plotted against the rotation speed Ω. Apart from the initial conditions at $\Omega=0$ (see below), the initial conditions for each value of Ω were obtained from the immediately preceding value. For a given value of Ω, a single point corresponds to a steady state and a finite number of points corresponds to a periodic vibration. The greater the distance between these points, the greater the amplitude of the oscillation.

In each panel, the *fixed*-ball configuration is indicated by circles. Here the balls were fixed at $\phi_1(t)=\pi/3+r_b$, $\phi_2(t)=\pi+r_b$ and $\phi_3(t)=4\pi/3+r_b$, for all $t>0$. The *coincident* configuration is indicated by crosses. Here the initial positions of the balls at $\Omega=0$ were chosen to already lie close to the coincident configuration, i.e. $\phi_1(0)=\pi/3+r_b$, $\phi_2(0)=5\pi/3-r_b$ and $\phi_3(0)=2\pi$. These initial conditions were chosen because, experimentally, the balls reach these positions after instability at a high speed. Moreover, the configuration persists as the speed is subsequently reduced. Therefore, in our simulations, when increasing the speed from zero, we must start the balls close to this coincident configuration. Finally, a *free*-ball configuration is indicated by squares. Here the initial positions of the balls at $\Omega=0$ were fixed at $\phi_1(0)=\pi/3+r_b$, $\phi_2(0)=\pi+r_b$ and $\phi_3(0)=5\pi/3+r_b$. These initial positions were chosen to model the experimentally observed positions of the balls immediately after the motor was turned on. After the long transient period of $t=10\ 000$, the balls are seen to stabilize in a free-ball configuration with steady-state positions $\phi_1\approx\pi/3+r_b$, $\phi_2\approx\pi+r_b$ and $\phi_3=2\pi-r_b$. In other words, the first two balls come to rest at a small distance away from their lagging partitions, while the third ball comes to rest against its leading partition. This is slightly different from what was observed experimentally, where the first two balls were shown to stay close to, but move slightly away from, their lagging partitions with the third ball coming to rest at $\phi_3\approx2\pi$. We believe that, in the experiment, the balls may be subject to additional stiction forces (van de Wouw *et al.* 2005). Such effects are not incorporated in our current model.

After the long transient period, the vibration results shown in each panel are qualitatively the same. The coincident-ball configuration (squares) is shown to produce the most vibration, followed by the free- and fixed-ball configurations, respectively. Both the free- and fixed-ball configurations are seen to undergo instabilities (highlighted by a number of points for a given value of Ω) as Ω is increased. Interestingly, this instability is shown to occur at increasingly higher values of Ω as β is increased.

In our experiments, we observed that the free-ball configuration became unstable at a rotation frequency of approximately 11.5 Hz. Given that the resonant frequency was measured to be 29.5 Hz, this corresponds to an instability at $\Omega\approx0.39$; thus suggesting that the internal damping in our experiments corresponds to a value of β of order one. Furthermore, in experiments, after this instability the balls moved to the coincident-ball configuration. This is not observed in our numerical investigations. Instead, the free-ball configuration is

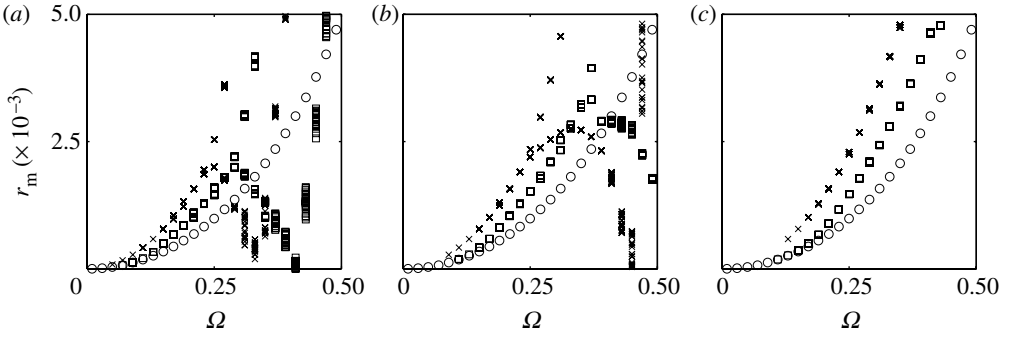

Figure 14. Numerical bifurcation diagrams showing extrema of the radial displacement versus rotation speed. Bifurcation diagrams obtained by numerical integration showing the extrema r_{m} of the radial vibration $r=\sqrt{x^2+y^2}$ against rotation speed Ω. Parameters were fixed at $\zeta=1.4027\times10^{-5}$, $\delta=0.0148$ and $\mu=0.011$; and (*a*) $\beta=0.1$, (*b*) $\beta=0.3$ and (*c*) $\beta=1.0$. (Circles, fixed-ball configuration; squares, free-ball configuration; and crosses, coincident-ball configuration.) Note that $\Omega\in[0,0.5]$ corresponds to a physical rotor speed of $\omega\in[0,14.75]$ Hz.

shown to destabilize to more complex dynamics which still do not reach the level of vibration of the coincident-ball configuration. Specifically, these dynamics correspond to each ball repeatedly impacting its front and back facing partitions.

7. Conclusions

The aim of the this paper has been to take the earlier bifurcation studies of Chung & Ro (1999), Adolfsson (2001) and Green *et al.* (2006*a*) and draw practical conclusions. To this end, we have designed and built an experimental rig. This rig is capable of assessing the suitability of automatic dynamic balancers at improving the vibration characteristics of eccentric rotors that are below their fundamental resonance frequency. The experiments repeatedly identified two steady-state configurations of the balls. One configuration was shown to add as much mass as was possible, subject to the partition constraints, to the imbalance. This configuration was analogous to the coincident steady state of the ADB without the partitions. The second configuration corresponded to all balls coming to rest away from a partition. This was shown to slightly add to the imbalance for the majority of rotation speeds. However, measurements repeatedly showed a reduction in the imbalance, and a lower radial vibration than for a fixed-ball configuration, for the lowest rotation speeds investigated. Bifurcation diagrams obtained by numerical integration of the equations of motion describing this impacting system revealed similar results. In particular, numerical simulation confirmed the existence of a free-ball configuration, similar to the one identified in the experiments. We believe that the discrepancies between our numerical and experimental results are due to stiction forces, which are not currently incorporated into our model.

The simplest conclusion from these results is that, despite the existence of various equilibrium positions of the balls which could improve the eccentric vibrations in theory, the ADB does not help for such rotation speeds. While this

conclusion may appear somewhat negative, there are several important steps we have established in understanding the consequences of the nonlinear dynamical analysis on the design of ADBs.

First, we have investigated the effects of using more than two balls. The results are mixed. Increasing the number of balls increases the number of possible equilibrium states and also the number of internal degrees of freedom within the perfectly balanced state. Intuitively, these extra equilibria may give rise to more robustness and larger basins of attraction of the balanced state, and we have found some evidence to support this. However, increasing the number of balls appears to decrease the range of parameter values at which balance is possible. Further detailed comparison would be necessary for particular rotor geometry and operating rotation speeds to ascertain how many balls would be optimal.

Second, we have established the advantages of the use of partitioned ball races, with one ball in each partition. This simple modification to the simplest design obviates the need for complex release mechanisms that clamp the balls to the rotor until a desired rotation speed is reached.

Third, we have established partial agreement between our experimental results and simulations of the numerical model. Note that bifurcation studies of the problem containing partitions are not straightforward due to the presence of non-smooth impacting behaviour. Future work may use recently developed bifurcation software for impacting systems which will allow the detection of non-smooth bifurcations (Budd *et al.* 2005) in addition to steady-state and Hopf bifurcations that occur in the smooth system.

It has been beyond the scope of this paper to investigate all possible nonlinear dynamics of the ADB with more than two balls, either with or without partitions. Green *et al.* (2006*a*,*b*) have shown the necessity of these studies in understanding the actual behaviour of the system, including transient effects and multistability between competing stable states. These studies are likely to be especially important for supercritical rotors (for which $\Omega > 1$) which we have shown are likely to be the only kinds of system for which an ADB might be effective. The building of a lightweight, low bearing stiffness, experimental rig would appear to be pressing, since our current experimental set-up is not able to access such rotation speeds.

Another important issue worthy of further study is to look at the combined effects of viscous damping, stiction and impacts with partitions in the ball race. It is probable that stiction could in fact be playing a role in the experiments described in this paper, resulting in some of the differences with the numerical simulations. Other geometries are also possible for the implementation of the balancing masses, e.g. pendula or paddles mounted at separate axial positions on the shaft (Horvath & Flowers 2005). It is clear from the bifurcation studies that ball race damping is one of the key parameters governing the existence and robustness of the stable balanced state and more modelling effort needs to put into on characterizing how this damping arises in practice.

Finally, we have looked only at the use of ADBs to balance eccentric rotors. Work in progress is looking at using multiple ADB discs which might also correct for vibrations due to couple imbalance.

The authors would like to thank Jorge Galán Vioque for helpful discussions, Clive Rendall and Tony Griffith for their continued technical support while designing, building and running the experimental rig, and Marian Wiercigroch for his comments on an earlier draft. K.G. was funded

by the EPSRC grant GR/535684/01. M.I.F. gratefully acknowledges the support of the Royal Society through a Royal Society-Wolfson Research Merit Award. The visit of A.M.M. to Bristol was made possible through the EU Socrates/Erasmus scheme.

References

Adolfsson, J. 2001 Passive control of mechanical systems: bipedal walking and autobalancing. PhD thesis, Royal Institute of Technology, Stockholm.

Budd, C., di Bernardo, M., Champneys, A. R., Nordmark, A. B., Olivar, G. & Piiroinen, P. T. 2005 Bifurcations in nonsmooth systems. BCANM technical report. See http://www.enm.bris.ac.uk/anm/preprints/2005r04.html.

Chung, J. & Ro, D. S. 1999 Dynamic analysis of an automatic dynamic balancer for rotating mechanisms. *J. Sound Vib.* **228**, 1035–1056. (doi:10.1006/jsvi.1999.2456)

Dhooge, A., Govaerts, W., Kuznetsov, Y. A., Mestrom, W., Riet, A. M. & Sautois, B. 2004 MATCONT and CL_MATCONT: continuation toolboxes in MATLAB. See http://www.matcont.ugent.be.

Ernst, H. 1951 Automatic precision balancing. *Mach. Des.* **N23**, 107–114.

Green, K. 2005 Analysis of an automatic dynamic balancing mechanism for eccentric rotors. In *Fifth EUROMECH Nonlinear Dynamics Conference* (eds D. H. van Campen, M. D. Lazurko & W. P. J. M. van den Oever).

Green, K., Champneys, A. R. & Lieven, N. J. 2006*a* Bifurcation analysis of an automatic dynamic balancing mechanism for eccentric rotors. *J. Sound Vib.* **291**, 861–881. (doi:10.1016/j.jsv.2005.06.042)

Green, K., Champneys, A. R. & Friswell, M. I. 2006*b* Analysis of the transient response of an automatic dynamic balancer for eccentric rotors. *Int. J. Mech. Sci.* **48**, 274–293. (doi:10.1016/j.ijmecsci.2005.09.014)

Horvath, R. & Flowers, G. T. 2005 Passive balancing for rotor systems using pendulum balancers. In *Proc. 20th ASME Int. Biennial Conf. on Mechanical Vibration and Noise.*

Huang, W.-Y., Chao, C.-P., Kang, J.-R. & Sung, C.-K. 2002 The application of ball-type balancers for radial vibration reduction of high-speed optic drives. *J. Sound Vib.* **250**, 415–430. (doi:10.1006/jsvi.2001.3921)

Hwang, C.-H. & Chung, J. 1999 Dynamic analysis of an automatic ball balancer with double races. *JSME Int. J. Ser. C* **42**, 265–272.

Jeffcott, H. H. 1919 The lateral vibration of loaded shafts in the neighbourhood of a whirling speed—the effect of want of balance. *Philos. Mag.* **6**, 304–314.

Kim, W. & Chung, J. 2002 Performance of automatic ball balancers on optical disc drives. *Proc. Inst. Mech. Eng. Part C: J. Mech. Eng. Sci.* **216**, 1071–1080. (doi:10.1243/095440602761609443)

Kuznetsov, Y. A. 1997 *Elements of applied bifurcation theory.* Berlin, Germany: Springer.

Lee, J. & Van Moorhem, W. K. 1996 Analytical and experimental analysis of a self-compensating dynamic balancer in a rotating mechanism. *ASME J. Dyn. Syst. Meas. Control* **118**, 468–475.

Majewski, T. 1987 Synchronous vibration eliminator for an object having one degree of freedom. *J. Sound Vib.* **112**, 401–413. (doi:10.1016/S0022-460X(87)80107-4)

Rajalingham, R. & Rakheja, S. 1998 Whirl suppression in hand-held power tool rotors using guided rolling balancers. *J. Sound Vib.* **217**, 453–466. (doi:10.1006/jsvi.1998.1780)

Ryzhik, B., Duckstein, H. & Sperling, L. 2004*a* Partial compensation of unbalance by one- and two-plane automatic balancing devices. *Int. J. Rotating Mach.* **10**, 193–201. (doi:10.1155/S1023621X0400020X)

Ryzhik, B., Sperling, L. & Duckstein, H. 2004*b* Auto-balancing of anisotropically supported rigid rotors. *Technische Mechanik* **24**, 37–50.

Sharp, R. S. 1975 An analysis of a self-balancing system for rigid rotors. *J. Mech. Eng. Sci.* **17**, 186–189. (doi:10.1243/JMES_JOUR_1975_017_027_02)

Thearle, E. 1932 A new type of dynamic-balancing machine. *Trans. ASME* **54**, 131–141.

van de Wouw, N., van den Heuvel, M. N., van Rooij, J. A. & Nijmeijer, H. 2005 Performance of an automatic ball balancer with dry friction. *Int. J. Bifurcat. Chaos* **15**, 65–82. (doi:10.1142/S0218127405012016)